

AutoRegressive Generation with B-rep Holistic Token Sequence Representation

Jiahao Li¹ Yunpeng Bai² Yongkang Dai¹ Hao Guo¹ Hongping Gan¹
Yilei Shi^{1*}

¹Northwestern Polytechnical University ²National University of Singapore

{lijiahao142857, daiyongkang, guoh0215}@mail.nwp.edu.cn

{ganhongping, yilei.shi}@nwp.edu.cn, bai-yunpeng99@u.nus.edu

Abstract

Previous representation and generation approaches for the B-rep relied on graph-based representations that disentangle geometric and topological features through decoupled computational pipelines, thereby precluding the application of sequence-based generative frameworks, such as transformer architectures that have demonstrated remarkable performance. In this paper, we propose BrepARG, the first attempt to encode B-rep’s geometry and topology into a holistic token sequence representation, enabling sequence-based B-rep generation with an autoregressive architecture. Specifically, BrepARG encodes B-rep into 3 types of tokens: geometry and position tokens representing geometric features, and face index tokens representing topology. Then the holistic token sequence is constructed hierarchically, starting with constructing the geometry blocks (i.e., faces and edges) using the above tokens, followed by geometry block sequencing. Finally, we assemble the holistic sequence representation for the entire B-rep. We also construct a transformer-based autoregressive model that learns the distribution over holistic token sequences via next-token prediction, using a multi-layer decoder-only architecture with causal masking. Experiments demonstrate that BrepARG achieves state-of-the-art (SOTA) performance. BrepARG validates the feasibility of representing B-rep as holistic token sequences, opening new directions for B-rep generation.

1. Introduction

Boundary Representation (B-rep) [29] is a fundamental paradigm in Computer-Aided Design (CAD) for representing solid models. Recent progress in B-rep data generation [8, 12, 18, 35] has advanced the automation and learning of CAD modeling processes. However, B-rep structures are inherently complex: they combine heterogeneous ge-

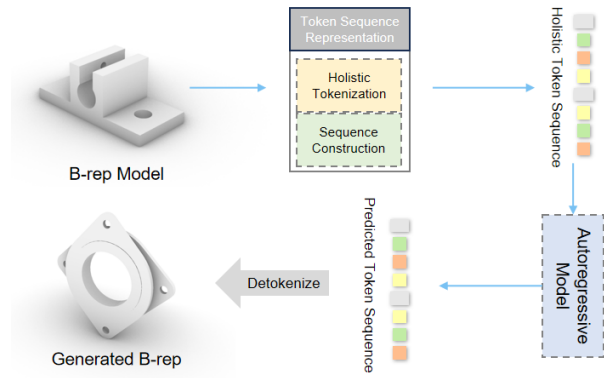


Figure 1. *BrepARG* is the first approach to encode the geometry and topology of a B-rep into a holistic token sequence, enabling efficient modeling and generation via an autoregressive model.

ometric primitives (parametric faces, edges, and vertices) within hierarchical topological dependencies. This heterogeneity makes it difficult to encode B-rep data in a direct, holistic form suitable for deep generative modeling.

Existing methods fall short in representing geometric and topological features holistically. They generally rely on stage-wise learning paradigms that separately model geometry and topology [12, 18, 35], or employ multi-component architectures for different elements [8]. Such designs lead to fragmented representations and increased model complexity. Moreover, graph-based formulations [8, 35] constrain the use of efficient transformer-based architectures that require sequential inputs, while multi-stage approaches [12, 18] limit the model’s ability to capture the full heterogeneity and interdependence inherent in B-rep.

To holistically represent B-rep, in this work, we propose a **B-rep AutoRegressive Generation (BrepARG)** framework, based on a novel *holistic token sequence representation*. The core idea is to encode the complete geometry and topology of a B-rep as a single token sequence, enabling direct autoregressive modeling (see Figure 1). The token se-

*Corresponding author.

quence representation comprises holistic tokenization and sequence construction (see Figure 2). For tokenization, geometry and topology of faces and edges are discretized separately, forming 3 types of tokens. The geometry primitives, i.e., faces and edges, are UV-sampled and tokenized into *Geometry Tokens* by mapping their vector-quantized variational autoencoder (VQ-VAE) encoder latents to codebook indices via nearest neighbor search. The 3D positions, i.e., bounding boxes, are encoded into *Position Tokens* through a newly designed *uniform scalar quantization* algorithm. The topology information is explicitly represented through shared *Face Index Tokens*. For sequence construction, we first construct geometry blocks, each consisting of all 3 types of tokens and representing a face or an edge. Then we use a topology-aware sequentialization scheme to sequence all face and edge blocks respectively, forming the face and edge block sequences, enforcing causal ordering while preserving local structural relationships. Finally, we assemble face block sequence and edge block sequence, together with necessary markers, to form the final holistic sequence representation.

To better leverage the powerful autoregressive framework, *BrepARG* then employs a transformer-based autoregressive model to learn the holistic geometric-topological token sequence via the next-token prediction task, thereby learning their joint distribution. This design enables the model to co-generate geometric shapes and topological connections in a single stream, achieving end-to-end autoregressive generation of B-rep sequences. Experiments demonstrate that *BrepARG* achieves state-of-the-art (SOTA) performance in B-rep generation while maintaining high efficiency, requiring only about 1.2 days to train on DeepCAD [32] with 4 NVIDIA H20 GPUs and around 1.5 seconds per B-rep for inference on a single RTX 4090. With *BrepARG*, we make the following contributions:

- We propose a novel ***holistic token sequence representation*** for B-rep, encoding both geometric and topological information into a single token sequence, addressing the long-standing fragmentation between geometry and topology in traditional approaches.
- We develop an ***autoregressive framework*** for B-rep generation that holistically learns geometric and topological structures through self-attention, eliminating multi-stage pipelines and improving efficiency.
- We conduct experiments to show that *BrepARG* achieves SOTA performance on B-rep generation tasks.

2. Related work

2.1. CAD Generation

Early CAD generation methods predominantly used Constructive Solid Geometry (CSG) [5, 13, 25, 26, 37, 38], constructing models via Boolean operations on simple primitives, which limits their ability to represent complex geometries.

Another line of work [4, 19, 32–34] learns parametric CAD command sequences that capture sketch structures, extrusion parameters, and action orderings to synthesize 3D shapes. Yet the development of this approach is currently limited by two main factors: 1) difficulty in supporting complex CAD design commands, 2) a persistent scarcity of high-quality, large-scale datasets.

2.2. B-rep Generation

B-rep represents objects by combining parametric geometric primitives with topological relationships, serving as a fundamental representation in industrial CAD. Prior work [3, 7, 10, 11, 16, 31] has studied B-rep classification and segmentation. For direct B-rep generation, [12, 35] employ multistage models for geometry learning and use multi-level pointer networks or tree structures to incrementally construct topology. DTGBrep [18] disentangles topology and geometry learning by employing separate networks to model topological structures and geometric primitives, respectively. [20] encodes the B-rep into a latent holistic feature of the face, yet decoding the topological relationships still relies on a deep neural network. [8] encodes B-rep structure as a 3D graph for diffusion while still employing multipipeline encoders for geometric elements.

2.3. Autoregressive Models for 3D Generation

In the field of large language models, the autoregressive next-token prediction paradigm has become the mainstream approach [2, 6, 14, 24, 30, 41], demonstrating remarkable performance and scalability. Recently, this paradigm has also been extended to 3D content generation, where key advances rely on effective serialization of 3D data. Existing methods primarily focus on point clouds [1, 22, 28, 36, 39] and meshes [17, 23, 27, 40, 43], using various ordering or encoding strategies for sequence modeling.

However, these approaches are difficult to directly apply to B-rep serialization due to the fundamental gap in data representation, and effective B-rep serialization methods for direct generation remain largely underexplored. The most related work, SolidGen [12], models faces, edges, and vertices in three separate stages and is limited to basic geometric primitives. In contrast, our holistic tokenization of the entire B-rep into a single sequence enables end-to-end autoregressive generation and extends support to more complex geometric elements, such as B-spline edges and faces.

3. Holistic Token Sequence Representation

The core challenge of holistic B-rep representation lies in the tight coupling between continuous, heterogeneous parametric geometry and discrete topology. To address this, we design a holistic token-sequence representation from two

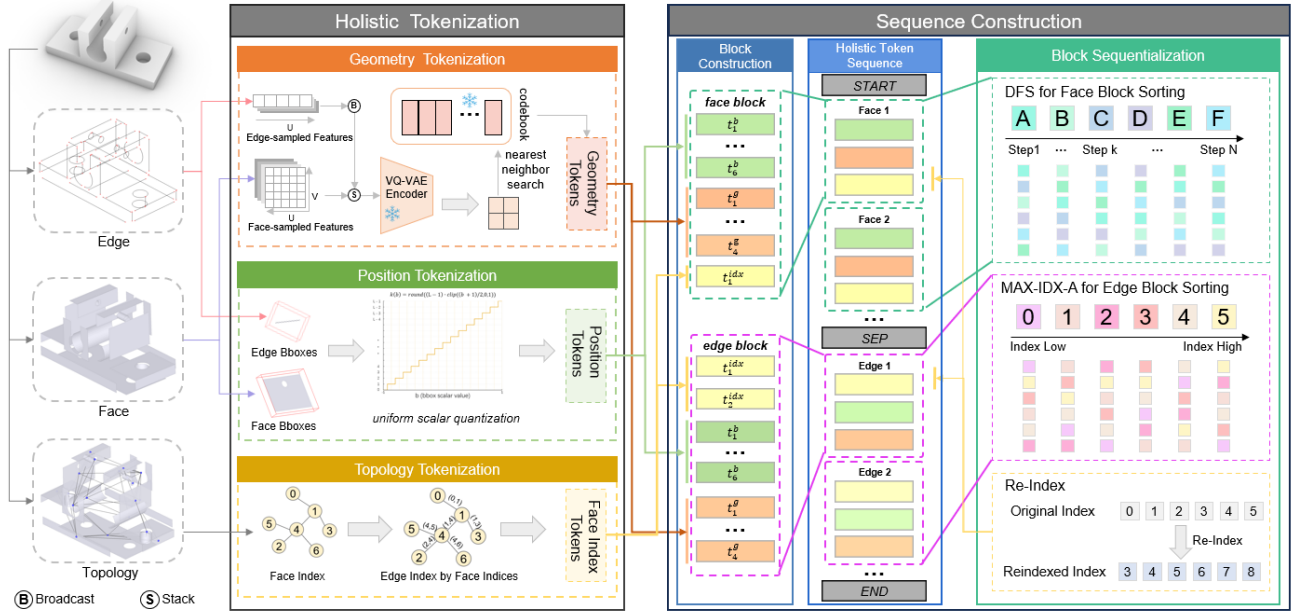


Figure 2. Our Holistic Token Sequence Representation comprises two parts: 1) **Holistic Tokenization**: *Geometry Tokens* are constructed by mapping VQ-VAE encoder latents to the codebook. *Position Tokens* are constructed by applying uniform scalar quantization to bounding boxes (Bboxes). *Face Index Tokens*, used for conveying topology information, are constructed by assigning an index to each face. 2) **Sequence Construction**: We first assemble face and edge blocks using the three token types above. These blocks are then ordered independently using DFS and the MAX-IDX-A algorithm. Finally, the ordered face and edge block sequences are concatenated with a separator and wrapped with start/end-of-sequence markers, producing the holistic token sequence representation of the entire B-rep model.

perspectives: holistic tokenization and sequence construction, as illustrated in Figure 2.

3.1. Holistic Tokenization

To form a holistic tokenization for B-rep, we need to tokenize geometry primitives (i.e., faces and edges) and topology. Thus, the holistic tokenization of B-rep comprises three components: 1) **Geometry Tokenization**, which tokenizes faces and edges; 2) **Position Tokenization**, which tokenizes the 3D positions (i.e., bounding boxes) of faces and edges in the B-rep for generation; 3) **Topology Tokenization**, which encodes the topology of B-rep into tokens.

Geometry Tokenization. For geometric faces and edges, we construct learnable representations via regular sampling in the UV parameter domain. For each face, we build an evenly spaced UV grid and sample 32×32 points, forming a discrete representation $\mathbf{F} \in \mathbb{R}^{32 \times 32 \times 3}$. For each edge, we uniformly sample 32 points along the U -axis, forming a discrete representation $\mathbf{E} \in \mathbb{R}^{32 \times 3}$. To reduce the geometry token vocabulary and enable token reuse, we employ a unified VQ-VAE for both faces and edges based on a 2D convolutional U-Net architecture. To match the input dimensionality required by the 2D convolutional network, \mathbf{E} is broadcast to $\mathbf{E}' \in \mathbb{R}^{32 \times 32 \times 3}$. To balance quantization fi-

delity and codebook size, we downsample the sampled features by a factor of 16, yielding a 2×2 latent feature map composed of four latent vectors. Each latent vector is then mapped to the nearest codeword in the codebook through a nearest neighbor search, and the corresponding indices are used as quantized representations. Consequently, the four indices derived from each face and edge constitute our final *Geometry Tokens*.

Position Tokenization. It is crucial to provide 3D positional information for geometric primitives (i.e., faces and edges) during B-rep generation. However, the large number of bounding boxes makes it difficult to tokenize the positional data, which are represented by six scalar values $\mathbf{b} = [x_{\min}, y_{\min}, z_{\min}, x_{\max}, y_{\max}, z_{\max}] \in [-1, 1]^6$. We find that when a single codeword is used to represent an entire bounding box, the VQ-VAE degenerates into an n -means clustering process over a large sample space, thus failing to achieve sufficient geometric accuracy. We also observe that splitting a bounding box into multiple sub-vectors and quantizing them into separate codewords still yields limited reconstruction fidelity, as the large data volume makes it difficult for the model to learn a precise mapping from continuous coordinates to discrete tokens.

To achieve a more stable mapping to token represen-

tations and higher quantization precision, we novelly tokenize bounding boxes by applying a coordinate-wise *uniform scalar quantization* method, where each coordinate is quantized using mathematical formulas to directly map the values to discrete token indices. Specifically, for each coordinate b_j ($j \in \{1, \dots, 6\}$), we first normalize and clip it to $[0, 1]$ to obtain \tilde{b}_j . We then scale it onto an L -level uniform grid and round to the nearest integer to obtain a discrete index:

$$k_j = \text{round}((L-1)\tilde{b}_j) \in \{0, \dots, L-1\}. \quad (1)$$

This procedure is applied independently to all six coordinates, yielding 6 *Position Tokens* (k_1, \dots, k_6). The corresponding dequantization uses a linear mapping:

$$b_j = \frac{2k_j}{L-1} - 1. \quad (2)$$

Topology Tokenization. The essence of topological relationships lies in representing the connectivity among geometry primitives. Therefore, as long as connectivity can be expressed, topology can be tokenized. Thus, our topology tokenization strategy employs a labeling approach on tokens derived from geometric primitives to encode the adjacency relationships between edges and faces.

Specifically, all closed face regions and boundary edges are split along their seams to ensure that each edge serves as the boundary between two distinct faces, and that the endpoints of each edge correspond to different vertices. By implicitly representing vertices through edge endpoints, we focus on faces and their adjacency topology. Firstly, we append a face index to each face as a unique identifier for subsequent references. Then, we append two face indices to each edge to explicitly encode face-edge adjacency.

3.2. Sequence Construction

We construct sequence representation hierarchically. We first construct geometry blocks for each face and edge with previously tokens. Then, two types of geometry blocks are respectively ordered with designed algorithms. Finally, we assemble the final holistic sequence representation.

Geometry Block Construction. We design two geometry blocks respectively for faces and edges. Each *face block* f_i contains three types of tokens: 6 consecutive Position Tokens t_i^p , 4 consecutive Geometry Tokens t_i^g , and a *Face Index Token* t_i^{idx} , formulated as:

$$f_i = [(t_1^p, \dots, t_6^p), (t_1^g, \dots, t_4^g), t_i^{idx}] \quad (3)$$

Each *edge block* e_j begins with 2 *Face Index Tokens* t_k^{idx} , corresponding to the pair of faces that share this edge. In this way, we explicitly encode the topology, i.e., the connectivity of two faces and one edge. The *Face Index Tokens*

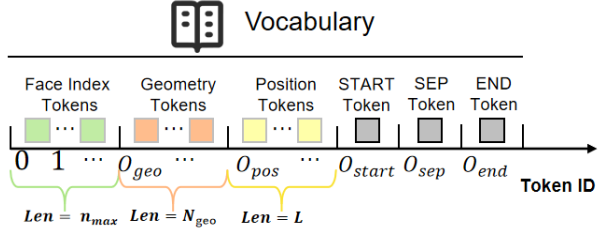


Figure 3. Unified vocabulary. Face Index, Geometry, Position, and Special tokens (*START*, *SEP*, *END*) are unified into a nonoverlapping vocabulary via predefined offsets.

are followed by the 6 Position tokens t_i^p and 4 Geometry Tokens t_j^g . The whole *edge block* is formulated as:

$$e_j = [t_1^{idx}, t_2^{idx}, (t_1^p, \dots, t_6^p), (t_1^g, \dots, t_4^g)] \quad (4)$$

Geometry Block Sequentialization. In this section, we design a topology-aware sequentialization strategy for sequencing *face blocks* and *edge blocks*, respectively. When sequentializing geometric primitives with embedded topological information, arbitrary ordering may compromise the structural integrity of the original B-rep model. To mitigate this issue, we construct a causal and topology-aware sequence order. Faces are ordered by first selecting the highest-degree face and then performing a depth-first search (DFS) that prioritizes lower-degree neighbors, so as to place topologically adjacent faces closer together in the sequence, yielding the *face block* sequence S_f . Edges are then ordered according to the maximum adjacent face index in ascending order (MAX-IDX-A), ensuring that edges are placed near their associated faces, which tightens the attention span between faces and edges and alleviates long-range dependencies, forming the *edge block* sequence S_e . After sequencing, we follow GraphGPT [42] and re-index all *Face Index Tokens*, where a random integer $r \in [0, n_{\max}]$ is added and then taken modulo n_{\max} , with n_{\max} denoting the maximum face count across all B-rep models in the dataset. This operation randomizes the topology encoding for generalization.

Final Sequence Assembly. To simplify the decoding process during detokenization, we organize the holistic token sequence so that all face blocks are enumerated first, followed by all edge blocks, which can be defined as:

$$S = [\text{START}, S_f, \text{SEP}, S_e, \text{END}] \quad (5)$$

Here, *START*, *SEP*, and *END* are *Special Tokens* denoting the sequence start, the separator between face and edge subsequences, and the sequence end, respectively. S_f and S_e represent all face and edge blocks, respectively.

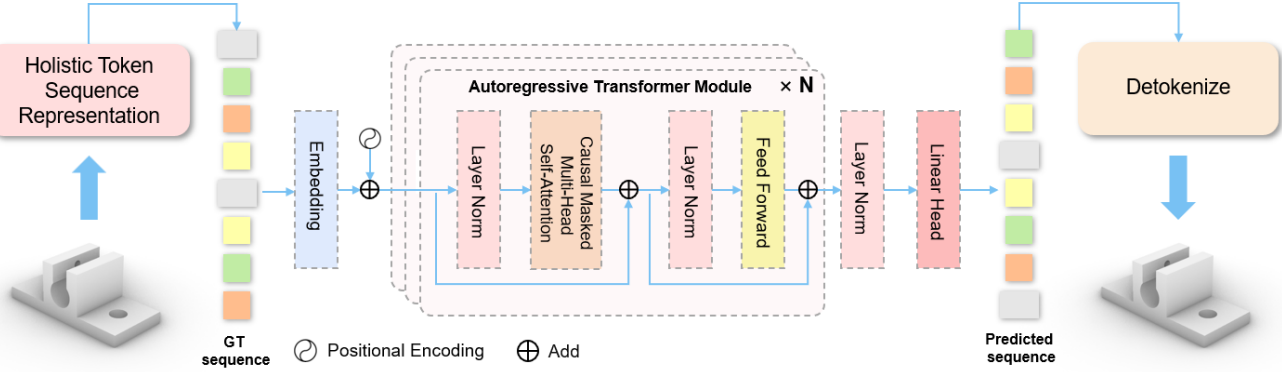


Figure 4. B-rep generation pipeline using a sequential generative model. The holistic token sequence of the B-rep is fed into an autoregressive, decoder-only Transformer for generation, and the predicted token sequence is detokenized to reconstruct the complete B-rep.

To embed discrete symbols from different sources, including *Face Index Tokens*, *Geometry Tokens*, *Position Tokens*, and *Special Tokens*, into a unified space without overlap, we adopt a segmented, non-overlapping linear token allocation scheme. In this design, each token subset is assigned a distinct starting offset along the global token index range, ensuring that all token types occupy disjoint index intervals. Specifically, let n_{\max} denote the maximum number of B-rep faces in the dataset, N_{geo} the size of the *VQ-VAE* codebook, and L the number of scalar quantization levels for bounding boxes. The segment offsets are defined as $o_{\text{geo}} = n_{\max}$, $o_{\text{pos}} = n_{\max} + N_{\text{geo}}$, and $o_{\text{spec}} = n_{\max} + N_{\text{geo}} + L$. This scheme merges the sub-vocabularies into a single continuous token space without index conflicts, as illustrated in Figure 3.

4. Generation Framework

The model *BrepARG* consists of two main components: 1) a *VQ-VAE* that compresses and quantizes the UV-sampled features of faces and edges into a shared codebook, and 2) an autoregressive training process based on a decoder-only transformer under teacher forcing, using the holistic token sequence representation (see Section 3 for details). Finally, we introduce a post-processing algorithm that detokenizes the generated sequences to reconstruct the complete B-rep model.

4.1. Face-Edge VQ-VAE

To obtain discrete representations of geometric information for faces and edges, we employ a *VQ-VAE* model built upon a 2D convolutional U-Net backbone. Given an input $\mathbf{x} \in \mathbb{R}^{32 \times 32 \times 3}$ (geometric features of faces or edges, \mathbf{F} or \mathbf{E}' ; see Section 3.1), the encoder downsamples it by a factor of 16 to produce a latent feature map $\mathbf{z}_e \in \mathbb{R}^{2 \times 2 \times 128}$. Then a 1×1 pointwise convolution linearly projects \mathbf{z}_e to 64 channels, yielding $\mathbf{z}'_e \in \mathbb{R}^{2 \times 2 \times 64}$ to match the dimensionality of the codebook.

Each latent vector in \mathbf{z}'_e is then mapped to its nearest codeword in the codebook through a nearest neighbor search, producing the quantized representation $\mathbf{z}_q \in \mathbb{R}^{2 \times 2 \times 64}$. The decoder reconstructs the input features as $\hat{\mathbf{x}} = D(\mathbf{z}_q)$, and the reconstruction loss is computed between \mathbf{x} and $\hat{\mathbf{x}}$ as $\mathcal{L}_{\text{rec}} = \|\mathbf{x} - \hat{\mathbf{x}}\|_2^2$.

To mitigate codebook collapse during training, we follow the codebook restart strategy of *CVQ-VAE* [44]: a feature-pool-driven online reinitialization together with probabilistic nearest neighbor sampling is used to revive low-usage codebook entries. This design improves codebook utilization and provides a more robust discrete representation for subsequent autoregressive modeling.

4.2. Sequential Generative Model

To effectively capture the geometric and topological regularities within holistic token sequences, we employ a decoder-only transformer architecture equipped with causal masking to perform autoregressive next-token prediction, as illustrated in Figure 4. Specifically, we define the training dataset as $\mathcal{D} = \{\mathbf{S}^{(n)}\}_{n=1}^N$, where N is the total number of training sequences and each $\mathbf{S} = (t_1, t_2, \dots, t_T)$ contains T discrete tokens $t_i \in V$, with V denoting the token vocabulary. Each token is embedded into a d -dimensional vector with added discrete positional information, yielding a representation $\mathbf{e}(t_i) \in \mathbb{R}^d$. The resulting embeddings are processed by a decoder-only transformer backbone composed of stacked multi-head self-attention and feed-forward layers, which predicts the next token from the vocabulary conditioned on the preceding context. The transformer model, parameterized by θ , defines conditional probabilities $p_\theta(t_i | \mathbf{e}(t_{<i}))$, and the overall training objective is to maximize the joint probability of all sequences in the dataset:

$$\prod_{\mathbf{S} \in \mathcal{D}} \prod_{i=1}^{T(\mathbf{S})} p_\theta(t_i | \mathbf{e}(t_{<i}); \theta), \quad (6)$$

At inference time, tokens are generated autoregressively by sampling from $p_\theta(t_i | \mathbf{e}(t_{<i}))$, starting from the *START* token and continuing until the *END* token is produced.

4.3. Holistic Token Sequence Detokenization

For each generated holistic token sequence, the regular token-length design and SEP delimiters enable direct extraction of token blocks corresponding to individual faces and edges. Subsequently, we apply the VQ-VAE decoder and Equation 2 to detokenize the *Geometry Tokens* and *Position Tokens*, respectively, thereby recovering their geometric representations. Face-edge adjacency relationships are established via shared *Face Index Tokens*, which further enables the construction of face–face adjacency (as each edge connects two faces). To infer vertex information and reconstruct the B-rep model, we introduce a novel post-processing algorithm. First, we treat the endpoints of each edge as candidate vertices. Then, using a union-find-based greedy clustering approach, we iteratively merge the closest candidate points from different edges within each face boundary based on geometric proximity and local loop topology, while ensuring global consistency by unifying shared vertex groups across faces. Finally, each vertex is determined as the centroid of its constituent candidate points, resulting in a complete and unique vertex list, edge–vertex connectivity, and loop structures. The resulting geometry and topology are seamlessly stitched into a valid B-rep solid using OpenCascade’s sew function.

5. Experiment

5.1. Experiment Setup

Datasets. We use three datasets for training and evaluation. The DeepCAD dataset [32] is employed for unconditional generation, ablation studies, and efficiency evaluation, while the Furniture dataset [35] is used for class-conditioned generation. Both datasets are filtered following the same strategy as DTGBrepGen [18], removing B-rep models with more than 50 faces or with any single face containing over 30 edges. After filtering, the resulting sets contain 80,509 DeepCAD B-reps and 1,065 Furniture B-reps. ABC dataset [15] is used for unconditional generation. We extend the above filtering criteria by additionally excluding simple CAD models with fewer than 10 faces, yielding 105,798 valid B-reps.

Network architecture. *Quantization & codebooks.* We apply *uniform scalar quantization* (see Equation 1) with $L = 2,048$ levels. The VQ-VAE uses a codebook of size 4,096 on the DeepCAD dataset, 8,192 for the more complex ABC dataset. The network comprises 5 convolutional encoder blocks and 5 symmetric decoder blocks: the first four encoder blocks perform downsampling sequentially, while the last block extracts features. The output channels at each

stage are 32, 64, 128, 256, and 512, enabling progressive compression and abstraction of the input features.

Sequential generative model. For sequence generation, we use a decoder-only transformer with 8 layers and 8 attention heads. Each layer has an embedding dimension of 256 and a feed-forward hidden dimension of 1,024.

Training. VQ-VAE. During the VQ-VAE training phase, we use the AdamW optimizer [21] with a learning rate of 1×10^{-4} , a weight decay of 1×10^{-6} , and batch sizes of 2,048 and 8,192 for the DeepCAD and ABC datasets, respectively. To improve training efficiency and stability, we utilize automatic mixed precision (AMP) and Distributed-DataParallel (DDP) for multi-GPU parallelization. On the DeepCAD dataset, the model is trained on 4 NVIDIA H20 GPUs, requiring approximately 12 hours.

Sequential generative model. During the sequential generative model training phase, we also use the AdamW optimizer with a learning rate of 1×10^{-3} , weight decay of 1×10^{-2} , and a batch size of 128. AMP and DDP are again employed for efficient multi-GPU training. On the DeepCAD dataset, the model is trained for 500 epochs using 4 NVIDIA H20 GPUs, which takes approximately 17 hours.

Inference. We adopt a probabilistic autoregressive sampling strategy to generate B-rep sequences. The generation process begins with an initial context prompt: unconditional generation starts from the *START* token, whereas conditional generation uses a category-specific token. At each iteration, the model predicts a probability distribution over the vocabulary conditioned on all previously generated tokens. We apply nucleus (top- p) sampling [9], which selects the next token from the smallest subset of the vocabulary whose cumulative probability is at least p . The sampling process terminates when the *END* token is generated or when the maximum sequence length is reached.

Evaluation metrics. Following BrepGen [35], we adopt both distributional and CAD-specific metrics for comprehensive evaluation. Distribution metrics include Coverage (COV), Minimum Matching Distance (MMD), and Jensen-Shannon Divergence (JSD). COV measures the proportion of reference samples that are matched by generated samples, based on nearest-neighbor matching with Chamfer distance. MMD computes the average Chamfer distance from each reference sample to its closest generated sample. JSD quantifies the Jensen-Shannon divergence between point cloud histograms of generated and reference sets. CAD metrics include Novelty, Uniqueness, and Validity. Novelty measures the proportion of generated samples not present in the training set hash table. Uniqueness evaluates the ratio of distinct samples after deduplication within the generated set. Validity measures the proportion of watertight, topologically consistent, and non-degenerate samples verified by a CAD kernel.

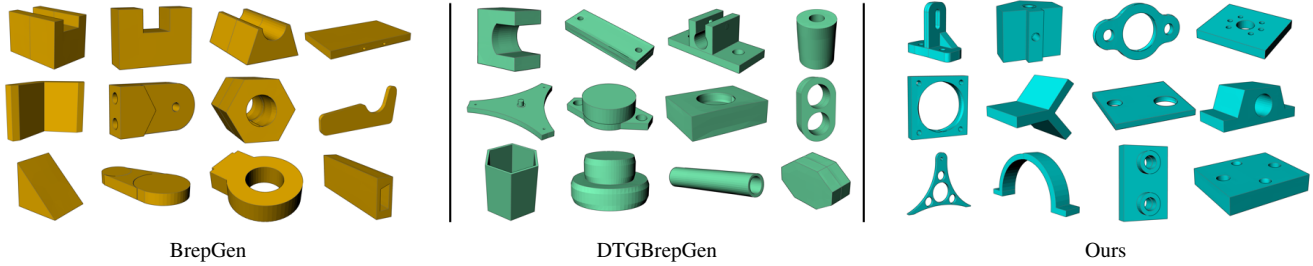


Figure 5. Qualitative comparison of B-rep models generated by BrepGen [35], DTGBrepGen [18], and our method (*BrepARG*) on the DeepCAD dataset.

Table 1. Comparison of unconditional generation results on the DeepCAD and ABC datasets. (MMD and JSD values are multiplied by 10^2 ; COV, Novel, Unique, and Valid are percentages.)

Method	DeepCAD					
	COV ↑	MMD ↓	JSD ↓	Novel ↑	Unique ↑	Valid ↑
DeepCAD	70.81	1.31	1.79	93.80	89.79	58.10
BrepGen	72.38	1.13	1.29	99.72	99.18	68.23
DTGBrepGen	74.52	1.07	1.02	99.79	98.94	79.80
Ours	75.45	0.89	1.02	99.82	99.80	87.60

Method	ABC					
	COV ↑	MMD ↓	JSD ↓	Novel ↑	Unique ↑	Valid ↑
DTGBrepGen	66.07	1.456	1.757	99.43	99.27	57.59
Ours	70.10	1.405	1.337	99.78	99.72	67.54

5.2. Unconditional Generation

To evaluate the performance of our model on unconditional generation, we conduct a comprehensive quantitative comparison with several baseline methods, including DeepCAD [32], BrepGen [35], and DTGBrepGen [18], using the DeepCAD dataset. For distribution metrics, we compute statistics over 3,000 generated B-rep models and 1,000 reference models, where each model is represented as a point cloud obtained by uniformly sampling 2,000 points. CAD metrics are directly evaluated on the 3,000 generated B-rep entities.

We report the mean of 10 independent runs, as shown in Table 1. Using nucleus (top- p) sampling with $p = 0.9$ for DeepCAD and $p = 0.8$ for ABC, our approach consistently

Table 2. Comparison of training and inference efficiency.

Method	Training Time	Training GPU	Inference Time	Inference GPU
BrepGen	7.5 days	H20 × 4	8.4 s	RTX4090 × 1
DTGBrepGen	3.0 days	H20 × 4	3.6 s	RTX4090 × 1
Ours	1.2 days	H20 × 4	1.5 s	RTX4090 × 1

Table 3. Results under different nucleus sampling thresholds p . Note that MMD and JSD values are multiplied by 10^2 ; COV, Novel, Unique, and Valid are percentages.

p	COV ↑	MMD ↓	JSD ↓	Novel ↑	Unique ↑	Valid ↑
0.95	76.10	0.8779	1.023	99.92	99.88	82.85
0.9	75.45	0.8869	1.017	99.82	99.80	87.60
0.8	73.71	0.9142	1.360	99.79	99.61	89.23
0.7	69.81	0.9594	2.370	99.21	98.62	89.51
0.6	63.50	1.0180	4.260	98.92	95.13	90.25

outperforms all baseline methods across all evaluation metrics. Notably, our model achieves a validity score of 87.6% on the DeepCAD dataset, demonstrating its strong ability to capture the geometric and topological structures of B-reps. As shown in Figure 5, qualitative comparisons further reveal that *BrepARG* generates more realistic and geometrically accurate B-rep models than the baselines.

Beyond generation quality, our generative model also demonstrates significant advantages in training and inference efficiency, as detailed in Table 2. Furthermore, we analyze the effect of different sampling strategies on generation outcomes. As shown in Table 3, by adjusting the p parameter in nucleus sampling, we can flexibly balance between generating more diverse models and achieving a higher proportion of valid B-rep outputs.

5.3. Class-conditioned Generation

We demonstrate the class-conditioned generation capability of *BrepARG* using a prefix-based conditioning strategy. During training, the *START* token at the beginning of each sequence is replaced with a class-specific token, enabling the model to learn class-aware autoregressive generation. At inference time, conditional generation is performed by prefixing the input sequence with the corresponding class token. Additional qualitative results are shown in Figure 6.

5.4. Failure Generation Cases

As shown in Figure 7, we observe several failure cases, which can be attributed to two primary factors: 1) preci-

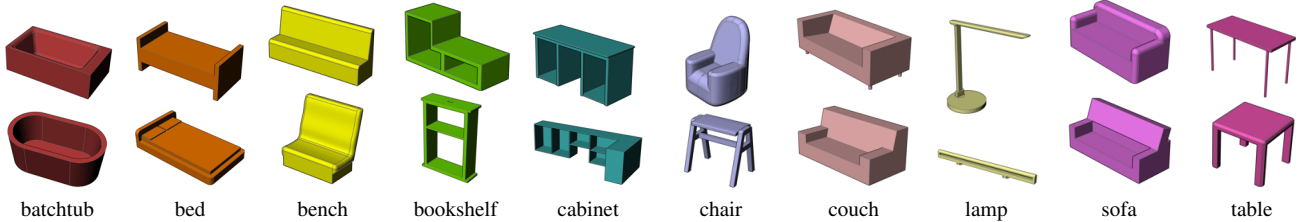


Figure 6. Class-conditioned generation. We showcase two representative B-rep samples for each category in the Furniture dataset, demonstrating our model’s ability for conditional generation.

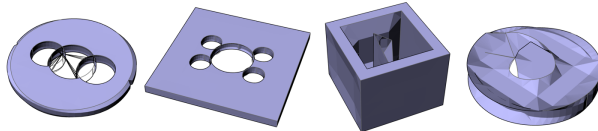


Figure 7. Failure cases generated by our method (*BrepARG*)

sion loss introduced by the *VQ-VAE* during quantization of geometric features of faces and edges, and 2) the increased complexity of modeling long autoregressive sequences. Future work will explore higher-fidelity geometric quantization schemes and more efficient autoregressive modeling strategies to further improve the stability and consistency of generated results.

5.5. Ablation Studies

To verify the effectiveness of the topology-aware sequentialization strategy in sequence construction, we conducted a systematic ablation study to evaluate various heuristic ordering schemes, including face ordering and edge ordering.

For face ordering, we evaluate 6 strategies covering different design principles, with a qualitative analysis of their combinations provided in the Appendix. A random ordering (RAND) serves as the baseline, while edge ordering is fixed to the maximum adjacent face index ascending (MAX-IDX-A) strategy, where edges are sorted in ascending order of the higher of their two adjacent face

Table 5. Ablation study of edge ordering strategies. Note that MMD and JSD values are multiplied by 10^2 ; COV, Novel, Unique, and Valid are percentages.

Method	COV \uparrow	MMD \downarrow	JSD \downarrow	Novel \uparrow	Unique \uparrow	Valid \uparrow
RAND	74.25	0.913	1.073	99.49	99.71	85.43
Ours	75.45	0.887	1.017	99.82	99.80	87.60

indices. Among topology-aware methods, we evaluate degree-ascending ordering (DEG-A), centroid-based ordering (ZYX; faces are sorted lexicographically by centroid coordinates in Z, then Y, then X), and spectral ordering (SS). We also explore traversal strategies starting from the highest-degree face, comparing breadth-first search (BFS) and our adopted depth-first search (DFS), both of which prioritize visiting low-degree neighbors. Results under consistent training and inference settings ($p = 0.9$) are summarized in Table 4.

For edge ordering strategies, we compare a random ordering (RAND) with our proposed ascending strategy, MAX-IDX-A. The results, obtained under consistent face ordering, training, and inference settings ($p = 0.9$), are summarized in Table 5.

The results show that the DFS-based traversal in face ordering and the MAX-IDX-A strategy in edge ordering jointly contribute to the overall performance. These findings highlight that the proposed topology-aware sequentialization effectively captures local connectivity patterns, leading to more coherent geometry and stable generation.

6. Conclusion

We propose *BrepARG*, the first framework that encodes the heterogeneous geometry and topology of B-rep into a holistic token sequence, reformulating B-rep generation as a sequence modeling task. This design enables sequence-based generation architectures, such as transformer, to jointly learn geometric details and topological constraints in a single process, effectively reducing multi-stage errors and computational overhead. Experimental results demonstrate that *BrepARG* achieves SOTA performance, paving a new direction for generative B-rep modeling.

Table 4. Ablation study of face ordering strategies. Note that MMD and JSD values are multiplied by 10^2 ; COV, Novel, Unique, and Valid are percentages.

Method	COV \uparrow	MMD \downarrow	JSD \downarrow	Novel \uparrow	Unique \uparrow	Valid \uparrow
RAND	71.10	0.9473	1.128	99.27	99.67	67.92
ZYX	74.82	0.9165	1.018	99.73	99.69	83.12
DEG-A	74.09	0.9059	1.290	99.52	99.35	82.98
SS	72.91	0.9551	1.403	99.58	99.19	79.38
BFS	74.65	0.9175	1.128	99.67	99.73	85.94
Ours	75.45	0.8869	1.017	99.82	99.80	87.60

References

[1] Guangyan Chen, Meiling Wang, Yi Yang, Kai Yu, Li Yuan, and Yufeng Yue. Pointgpt: Auto-regressively generative pre-training from point clouds. *Advances in Neural Information Processing Systems*, 36:29667–29679, 2023. [2](#)

[2] Aakanksha Chowdhery, Sharan Narang, Jacob Devlin, Maarten Bosma, Gaurav Mishra, Adam Roberts, Paul Barham, Hyung Won Chung, Charles Sutton, Sebastian Gehrmann, et al. Palm: Scaling language modeling with pathways. *Journal of Machine Learning Research*, 24(240):1–113, 2023. [2](#)

[3] Yongkang Dai, Xiaoshui Huang, Yunpeng Bai, Hao Guo, Hongping Gan, Ling Yang, and Yilei Shi. Brepformer: Transformer-based b-rep geometric feature recognition. In *Proceedings of the 2025 International Conference on Multimedia Retrieval*, pages 155–163, 2025. [2](#)

[4] Liyuan Deng, Yunpeng Bai, Yongkang Dai, Xiaoshui Huang, Hongping Gan, Dongshuo Huang, Hao Jiacheng, and Yilei Shi. Mamtiff-cad: Multi-scale latent diffusion with mamba+ for complex parametric sequence. In *Proceedings of the IEEE/CVF International Conference on Computer Vision*, pages 10517–10526, 2025. [2](#)

[5] Tao Du, Jeevana Priya Inala, Yewen Pu, Andrew Spielberg, Adriana Schulz, Daniela Rus, Armando Solar-Lezama, and Wojciech Matusik. Inversecsg: Automatic conversion of 3d models to csg trees. *ACM Transactions on Graphics (TOG)*, 37(6):1–16, 2018. [2](#)

[6] Abhimanyu Dubey, Abhinav Jauhri, Abhinav Pandey, Abhishek Kadian, Ahmad Al-Dahle, Aiesha Letman, Akhil Mathur, Alan Schelten, Amy Yang, Angela Fan, et al. The llama 3 herd of models. *arXiv e-prints*, pages arXiv–2407, 2024. [2](#)

[7] Jiajie Fan, Babak Gholami, Thomas Bäck, and Hao Wang. Neuronurbs: Learning efficient surface representations for 3d solids. *arXiv preprint arXiv:2411.10848*, 2024. [2](#)

[8] Hao Guo, Xiaoshui Huang, Yunpeng Bai, Hongping Gan, Yilei Shi, et al. Brepgriff: Lightweight generation of complex b-rep with 3d gat diffusion. In *Proceedings of the Computer Vision and Pattern Recognition Conference*, pages 26587–26596, 2025. [1, 2](#)

[9] Ari Holtzman, Jan Buys, Li Du, Maxwell Forbes, and Yejin Choi. The curious case of neural text degeneration. *arXiv preprint arXiv:1904.09751*, 2019. [6](#)

[10] Junhao Hou, Chenqi Luo, Feiwei Qin, Yanli Shao, and Xiaxuan Chen. Fus-gcn: Efficient b-rep based graph convolutional networks for 3d-cad model classification and retrieval. *Advanced Engineering Informatics*, 56:102008, 2023. [2](#)

[11] Pradeep Kumar Jayaraman, Aditya Sanghi, Joseph G Lambourne, Karl DD Willis, Thomas Davies, Hooman Shayani, and Nigel Morris. Uv-net: Learning from boundary representations. In *Proceedings of the IEEE/CVF conference on computer vision and pattern recognition*, pages 11703–11712, 2021. [2](#)

[12] Pradeep Kumar Jayaraman, Joseph G Lambourne, Nishkrit Desai, Karl DD Willis, Aditya Sanghi, and Nigel JW Morris. Solidgen: An autoregressive model for direct b-rep synthesis. *arXiv preprint arXiv:2203.13944*, 2022. [1, 2](#)

[13] Kacper Kania, Maciej Zieba, and Tomasz Kajdanowicz. Ucsg-net-unsupervised discovering of constructive solid geometry tree. *Advances in neural information processing systems*, 33:8776–8786, 2020. [2](#)

[14] Jared Kaplan, Sam McCandlish, Tom Henighan, Tom B Brown, Benjamin Chess, Rewon Child, Scott Gray, Alec Radford, Jeffrey Wu, and Dario Amodei. Scaling laws for neural language models. *arXiv preprint arXiv:2001.08361*, 2020. [2](#)

[15] Sebastian Koch, Albert Matveev, Zhongshi Jiang, Francis Williams, Alexey Artemov, Evgeny Burnaev, Marc Alexa, Denis Zorin, and Daniele Panozzo. Abc: A big cad model dataset for geometric deep learning. In *Proceedings of the IEEE/CVF conference on computer vision and pattern recognition*, pages 9601–9611, 2019. [6](#)

[16] Jinwon Lee, Changmo Yeo, Sang-Uk Cheon, Jun Hwan Park, and Duhwan Mun. Brepgrat: Graph neural network to segment machining feature faces in a b-rep model. *Journal of Computational Design and Engineering*, 10(6):2384–2400, 2023. [2](#)

[17] Jiabao Lei, Kewei Shi, Zhihao Liang, and Kui Jia. Armesh: Autoregressive mesh generation via next-level-of-detail prediction. *arXiv preprint arXiv:2509.20824*, 2025. [2](#)

[18] Jing Li, Yihang Fu, and Falai Chen. Dtgbrepgrn: A novel b-rep generative model through decoupling topology and geometry. In *Proceedings of the Computer Vision and Pattern Recognition Conference*, pages 21438–21447, 2025. [1, 2, 6, 7](#)

[19] Pu Li, Jianwei Guo, Xiaopeng Zhang, and Dong-Ming Yan. Secad-net: Self-supervised cad reconstruction by learning sketch-extrude operations. In *Proceedings of the IEEE/CVF Conference on Computer Vision and Pattern Recognition*, pages 16816–16826, 2023. [2](#)

[20] Yilin Liu, Duoteng Xu, Xingyao Yu, Xiang Xu, Daniel Cohen-Or, Hao Zhang, and Hui Huang. Hola: B-rep generation using a holistic latent representation. *ACM Transactions on Graphics (TOG)*, 44(4):1–25, 2025. [2](#)

[21] Ilya Loshchilov and Frank Hutter. Decoupled weight decay regularization. *arXiv preprint arXiv:1711.05101*, 2017. [6](#)

[22] Paritosh Mittal, Yen-Chi Cheng, Maneesh Singh, and Shubham Tulsiani. Autosdf: Shape priors for 3d completion, reconstruction and generation. In *Proceedings of the IEEE/CVF conference on computer vision and pattern recognition*, pages 306–315, 2022. [2](#)

[23] Charlie Nash, Yaroslav Ganin, SM Ali Eslami, and Peter Battaglia. Polygen: An autoregressive generative model of 3d meshes. In *International conference on machine learning*, pages 7220–7229. PMLR, 2020. [2](#)

[24] Alec Radford, Jeffrey Wu, Rewon Child, David Luan, Dario Amodei, Ilya Sutskever, et al. Language models are unsupervised multitask learners. *OpenAI blog*, 1(8):9, 2019. [2](#)

[25] Daxuan Ren, Jianmin Zheng, Jianfei Cai, Jiatong Li, Haiyong Jiang, Zhongang Cai, Junzhe Zhang, Liang Pan, Mingyuan Zhang, Haiyu Zhao, et al. Csg-stump: A learning friendly csg-like representation for interpretable shape parsing. In *Proceedings of the IEEE/CVF international conference on computer vision*, pages 12478–12487, 2021. [2](#)

[26] Gopal Sharma, Rishabh Goyal, Difan Liu, Evangelos Kalogerakis, and Subhransu Maji. Csgnet: Neural shape parser for constructive solid geometry. In *Proceedings of the IEEE conference on computer vision and pattern recognition*, pages 5515–5523, 2018. 2

[27] Yawar Siddiqui, Antonio Alliegro, Alexey Artemov, Tatiana Tommasi, Daniele Sirigatti, Vladislav Rosov, Angela Dai, and Matthias Nießner. Meshgpt: Generating triangle meshes with decoder-only transformers. In *Proceedings of the IEEE/CVF conference on computer vision and pattern recognition*, pages 19615–19625, 2024. 2

[28] Yongbin Sun, Yue Wang, Ziwei Liu, Joshua Siegel, and Sanjay Sarma. Pointgrow: Autoregressively learned point cloud generation with self-attention. In *Proceedings of the IEEE/CVF winter conference on applications of computer vision*, pages 61–70, 2020. 2

[29] Kevin J Weiler. *Topological structures for geometric modeling (Boundary representation, manifold, radial edge structure)*. Rensselaer Polytechnic Institute, 1986. 1

[30] BigScience Workshop, Teven Le Scao, Angela Fan, Christopher Akiki, Ellie Pavlick, Suzana Ilić, Daniel Hesslow, Roman Castagné, Alexandra Sasha Lucioni, François Yvon, et al. Bloom: A 176b-parameter open-access multilingual language model. *arXiv preprint arXiv:2211.05100*, 2022. 2

[31] Hongjin Wu, Ruoshan Lei, Yibing Peng, and Liang Gao. Aagnet: A graph neural network towards multi-task machining feature recognition. *Robotics and Computer-Integrated Manufacturing*, 86:102661, 2024. 2

[32] Rundi Wu, Chang Xiao, and Changxi Zheng. Deepcad: A deep generative network for computer-aided design models. In *Proceedings of the IEEE/CVF International Conference on Computer Vision*, pages 6772–6782, 2021. 2, 6, 7

[33] Xiang Xu, Karl DD Willis, Joseph G Lambourne, Chin-Yi Cheng, Pradeep Kumar Jayaraman, and Yasutaka Furukawa. Skexgen: Autoregressive generation of cad construction sequences with disentangled codebooks. *arXiv preprint arXiv:2207.04632*, 2022.

[34] Xiang Xu, Pradeep Kumar Jayaraman, Joseph G Lambourne, Karl DD Willis, and Yasutaka Furukawa. Hierarchical neural coding for controllable cad model generation. *arXiv preprint arXiv:2307.00149*, 2023. 2

[35] Xiang Xu, Joseph Lambourne, Pradeep Jayaraman, Zhengqing Wang, Karl Willis, and Yasutaka Furukawa. Brepgen: A b-rep generative diffusion model with structured latent geometry. *ACM Transactions on Graphics (TOG)*, 43(4):1–14, 2024. 1, 2, 6, 7

[36] Xinguang Yan, Liqiang Lin, Niloy J Mitra, Dani Lischinski, Daniel Cohen-Or, and Hui Huang. Shapeformer: Transformer-based shape completion via sparse representation. In *Proceedings of the IEEE/CVF conference on computer vision and pattern recognition*, pages 6239–6249, 2022. 2

[37] Fenggen Yu, Zhiqin Chen, Manyi Li, Aditya Sanghi, Hooman Shayani, Ali Mahdavi-Amiri, and Hao Zhang. Capri-net: Learning compact cad shapes with adaptive primitive assembly. In *Proceedings of the IEEE/CVF conference on computer vision and pattern recognition*, pages 11768–11778, 2022. 2

[38] Fenggen Yu, Qimin Chen, Maham Tanveer, Ali Mahdavi Amiri, and Hao Zhang. D²CSG: Unsupervised learning of compact csg trees with dual complements and dropouts. *Advances in Neural Information Processing Systems*, 36: 22807–22819, 2023. 2

[39] Xumin Yu, Lulu Tang, Yongming Rao, Tiejun Huang, Jie Zhou, and Jiwen Lu. Point-bert: Pre-training 3d point cloud transformers with masked point modeling. In *Proceedings of the IEEE/CVF conference on computer vision and pattern recognition*, pages 19313–19322, 2022. 2

[40] Jinzhi Zhang, Feng Xiong, and Mu Xu. G3pt: Unleash the power of autoregressive modeling in 3d generation via cross-scale querying transformer. *arXiv preprint arXiv:2409.06322*, 2024. 2

[41] Susan Zhang, Stephen Roller, Naman Goyal, Mikel Artetxe, Moya Chen, Shuhui Chen, Christopher Dewan, Mona Diab, Xian Li, Xi Victoria Lin, et al. Opt: Open pre-trained transformer language models. *arXiv preprint arXiv:2205.01068*, 2022. 2

[42] Qifang Zhao, Weidong Ren, Tianyu Li, Hong Liu, Xingsheng He, and Xiaoxiao Xu. Graphgpt: Generative pre-trained graph eulerian transformer. In *Forty-second International Conference on Machine Learning, ICML 2025, Vancouver, BC, Canada, July 13-19, 2025*. OpenReview.net, 2025. 4

[43] Ruowen Zhao, Junliang Ye, Zhengyi Wang, Guangce Liu, Yiwen Chen, Yikai Wang, and Jun Zhu. Deepmesh: Autoregressive artist-mesh creation with reinforcement learning. In *Proceedings of the IEEE/CVF International Conference on Computer Vision*, pages 10612–10623, 2025. 2

[44] Chuanxia Zheng and Andrea Vedaldi. Online clustered codebook. In *Proceedings of the IEEE/CVF International Conference on Computer Vision*, pages 22798–22807, 2023. 5